

Deviations in yield and ultimate tensile strength estimation with the Small Punch Test: numerical analysis of pre-straining and Bauschinger effect influence

Jose Calaf-Chica⁽¹⁾, Mario Sánchez Palomar⁽²⁾, Pedro Miguel Bravo Díez⁽³⁾, Mónica Preciado Calzada⁽⁴⁾

*E-mails: (1) Corresponding author, jcalaf@ubu.es ; (2) mario.sanchez.palomar@gmail.com; (3) pabravo@ubu.es; (4) mpreciado@ubu.es
Postal address: Departamento de Ingeniería Civil, Universidad de Burgos, Avenida Cantabria s/n, E09006 Burgos, Spain*

ABSTRACT

There is a growing interest on the Small Punch Test (SPT) and its many applications in a broad range of industries and sectors. The miniature volume of the SPT specimen eases the mechanical characterization of components and structures when standard tests are impracticable. But this miniature test is limited for one of its more constraining requirements: the material isotropy. Since this test subjects the material to triaxial stress and strain fields, isotropy is necessary to compare the resulted data from SPT with the standard tests, which generally show uniaxial stress fields. Another key element of this question is that initially, isotropic material can lose this property due to a cold pre-straining process and the existence of the Bauschinger effect. In this investigation, a numerical study with the finite element method was performed to understand the influence of pre-straining and the Bauschinger effect in yield strength and ultimate tensile strength estimation with the SPT. This study concludes that in the absence of isotropy, generated by a pre-straining, the SPT estimated a mean value of the principal yield strength components of the yield surface. It is also verified that presence of pre-straining in the SPT specimens invalidated their use to calculate the coefficients of the correlation equations for yield strength estimation.

Keywords: Small Punch Test, SPT, yield strength, ultimate tensile strength, pre-straining, Bauschinger effect.

Note: This research did not receive any specific grant from funding agencies in the public, commercial, or not-for-profit sectors.

1 Introduction

The energy sector has shown during the last years a growing interest on the miniature tests. They are characterization tests for a wide range of mechanical properties which use a very reduced material volume. In the nuclear sector, this test simplifies and facilitates the radiation embrittlement process of the specimens (Kim et al., 2005). Other industrial sectors consider these tests when there is a lack of material to mechanize a standard specimen (Kumar & Laha, 2017). In some cases, they could be considered as a quasi-non-destructive mechanical characterization test without necessarily compromising the structural integrity of the evaluated component (Guan et al., 2011). The Small Punch Test (SPT) is especially important within the wide range of miniature tests developed during the last decade. It stands out because of the array of evaluated materials with this test (ferrous and non-ferrous alloys (Gao et al., 2020; Li et al., 2020), polymers (Koga et al., 2020), ceramics (Rasche et al., 2014), etc.), and the wide selection of mechanical properties that can be evaluated with this test (Young's modulus (Calaf Chica et al., 2017), yield strength (Hähner et al., 2019), ultimate tensile strength (Altstadt et al., 2018), fracture toughness (Hurst et al., 2019), ductile-to-brittle transition temperature (W. Wang et al., 2020), creep (L. Y. Wang et al., 2019), etc.).

Figure 1(a) shows a schematic drawing of the SPT geometry and set-up, in which a disk of diameter equal to 8 mm and a thickness of 0.5 mm is clamped between two dies, lower and upper, and punched until failure by the vertical displacement of a 2.5 mm diameter sphere. In order to standardize this test, CEN published in 2006 the good practices code CWA 15627 (CEN Workshop Agreement, 2006) and the first European standard for the SPT is about to be published in late 2020. During the SPT testing the punch load and displacement are registered to obtain the SPT curve

(c) Intersections' method (Altstadt et al., 2018). This method uses the load P_i corresponding to a punch displacement of 0.645 mm.

Equations (1) to (5) represent the correlation equations used to link the obtained parameters from the SPT with the target mechanical property. For the specific case of yield strength estimation, the first three previously mentioned methods use equation (1), while the fourth method uses equation (2). The estimation of ultimate tensile strength uses: equation (3) for the maximum load method, equation (4) for the weighted maximum load method and equation (5) for the intersections' method. The coefficients α_1 , α_2 , β_1 and β_2 must be obtained empirically through SPTs and standard tensile tests of different materials with the least squares method.

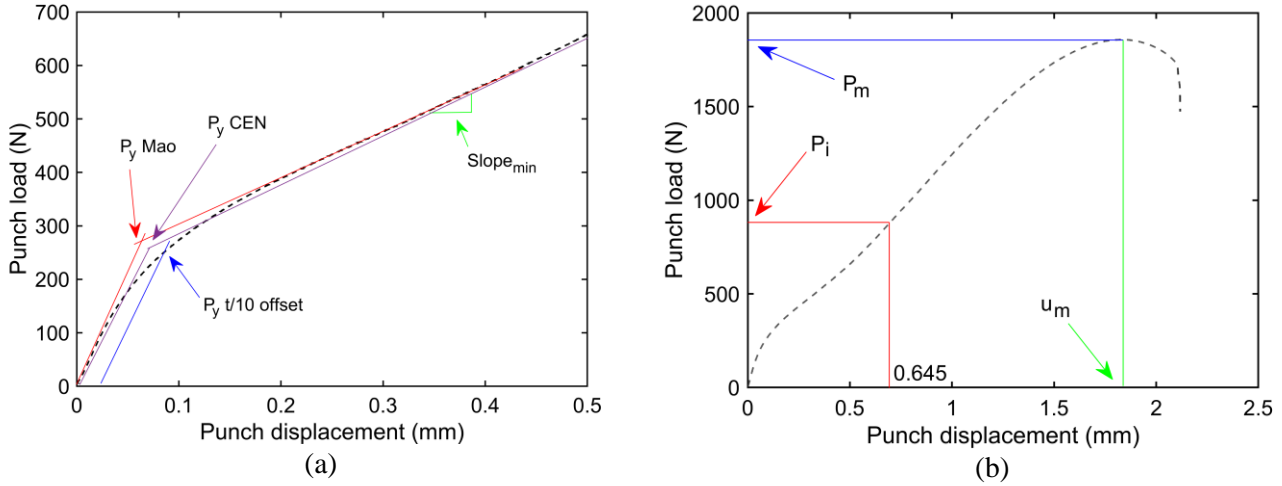


Figure 2. Parameters used in the correlation methods for (a) yield strength and (b) ultimate tensile strength estimation with the SPT

$$\sigma_y = \alpha_1 \frac{P_y}{t^2} + \alpha_2 \tag{1}$$

$$\sigma_y = \alpha_1 \frac{P_y}{t^2} + \alpha_2 \frac{Slope_{min}}{t} \tag{2}$$

$$\sigma_u = \beta_1 \frac{P_m}{t^2} + \beta_2 \tag{3}$$

$$\sigma_u = \beta_1 \frac{P_m}{tu_m} + \beta_2 \tag{4}$$

$$\sigma_u = \beta_1 \frac{P_i}{t^2} \tag{5}$$

where:

α_1 , α_2 , β_1 and β_2 are correlation coefficients obtained in the empirical linear regression, and t is the specimen thickness.

Research related with the SPT has shown more sophisticated ways to estimate the mechanical properties of materials. Neural networks (Abendroth & Kuna, 2003) and inverse finite element procedures (Husain et al., 2004) showed to be methodologies in order to directly estimate constitutive stress-strain curves of the tested materials. Although these methods show greater potential, their use is enough tricky to limit their applicability in a standard for mechanical characterization test in the industrial sector. That is the main reason the good practices code CWA 15627 does not include these sophisticated methodologies as an alternative.

One important point of all these correlation methods with the SPT is, that they rely on estimations of the mechanical property based on empirical correlation equations obtained from a previous comparison between standard tests and SPTs for similar materials. Thus, and for the specific case of mechanical properties inherent to the uniaxial tensile test, empirical data obtained from standard tests, that show uniaxial stress and strain fields, are correlated with parameters extracted from a test (the SPT) with triaxial stress and strain fields. This is the main reason for prefixing an essential requirement that any material which is mechanically characterized with the SPT must fulfill: its isotropy and homogeneity. Nevertheless, there are empirical investigations that analyze the influence of anisotropy in the estimation of mechanical properties with the SPT (Campitelli et al., 2005; Ma & Yoon, 2010; Okuda et al., 2009; Turba et al., 2012). It is important to note that an initially isotropic material can lose this property due to a previous plastic straining. The strain hardening results in an increment of yield strength for a direction and sense similar to the previous straining and a decrease of this mechanical property in the opposite sense (the Bauschinger effect). Metallic materials tend to show a combination of isotropic and kinematic hardenings. A greater weight of one or another hardening model determines the greater or lesser presence of the Bauschinger effect in the material. Thus, the presence of previous straining can remove the material isotropy and that could affect to the reliability of the SPT. Regarding the study of the influence of pre-straining in the estimation of mechanical properties with the SPT, there are few publications. Cuesta et al. (Cuesta & Alegre, 2012) noted that a 5000 series aluminum alloy with different pre-straining showed high deviations in the estimation of yield strength. It is for this reason that the correlation coefficients were recalculated based on these pre-strained specimens. Peng et al. (Peng et al., 2019) carried out a similar study with a stainless Steel AISI 360L. They tested tensile and SPT specimens of annealed material without pre-straining and with different pre-straining levels (tensile pre-straining of 5% and 10%). From the annealed specimens with no pre-straining they calculated the coefficients of the correlation equations for the estimation of yield strength. From the pre-strained specimens, they noted a significant deviation with respect the previously calculated correlation equation, being the deviation more prominent as the pre-straining levels were higher. Peng et al. concluded that the reliability of the SPT was compromised by pre-straining in the specimens.

In this investigation a numerical study with the finite element method (FEM) has been performed in order to understand the influence of pre-straining and the Bauschinger effect on the reliability of the SPT, both for the estimation of yield strength and ultimate tensile strength.

2 Materials and Methods

For the evaluation of the pre-straining and Bauschinger effect influence in the SPT, a kinematic Chaboche's model was used. **In a real metallic material, the strain hardening is, in a simple way, a combination of isotropic and kinematic models (mixed strain hardening). To discern empirically the higher or lower presence of each plastic behavior in a real material it is necessary to test the material with a complete loading cycle in a tension-compression test.** In this investigation a comparison between a pure isotropic behavior and a pure kinematic behavior was done. To make this possible, the coefficients of the Chaboche's model were selected to generate a strain hardening curve similar to a Ramberg-Osgood law (see equation (6)). Table 1 shows the selected mechanical properties of the Ramberg-Osgood isotropic model.

E (GPa)	ν	σ_y (MPa)	n
200	0.3	400	10

Table 1. Mechanical properties of the hypothetical material

$$\varepsilon_{true} = \frac{\sigma_{true}}{E} + \varepsilon_{offset} \left(\frac{\sigma_{true}}{\sigma_y} \right)^n \quad (6)$$

where:

$\varepsilon_{offset} = 0.002$ is the plastic strain of the offset yield point,

σ_{true} is the true stress,

ε_{true} is the true strain,

E is the Young's modulus,

σ_y is yield strength,
and n is the hardening coefficient.

The equation (7) shows the Chaboche's **back-stress** equation, where two back-stresses were selected in order to reach an equation that faithfully followed the Ramberg-Osgood model (6) with the coefficients included in Table 1. **Equation (8) shows the initial stress-strain curve using the Chaboche's kinematic model with an initial yield strength σ_{y0} .** The coefficients C_i and γ_i of the Chaboche's model were calculated with a non-linear least squares regression method, **considering the initial yield strength included in Table 1**, and Table 2 shows the obtained values and the coefficient of determination R^2

$$\sum_{i=1}^2 \alpha_i = \frac{C_1}{\gamma_1} (1 - e^{-\gamma_1 \varepsilon_p}) + \frac{C_2}{\gamma_2} (1 - e^{-\gamma_2 \varepsilon_p}) \quad (7)$$

$$\sigma = \sigma_{y0} + \sum_{i=1}^2 \alpha_i \quad (8)$$

n	C_1 (MPa)	γ_1	C_2 (MPa)	γ_2	R^2
10	8854	65.6	656	3.1	0.997

Table 2. Chaboche's coefficients determination

The SPT simulations were conducted with ANSYS v18.2 software. For the purpose of simulating the pre-straining process prior to the SPT, the specimen had an initial thickness different from the nominal ones of $t = 0.5$ mm. In a first step, the SPT specimen was deformed until it reached a target level of plastic strain, after which it returned elastically. The initial specimen thickness was established in an iterative process with the goal of reaching a specific value of plastic strain and a final specimen thickness equal to the nominal value of $t = 0.5$ mm. Once this first step was completed, SPT simulation was performed in this pre-strained specimen. The conducted simulations were: two cases with pre-straining in the specimen normal axis (y-axis), one with tensile pre-straining and another with compressive pre-straining; and two cases with pre-straining in an axis contained in the specimen plane (x-axis), also with tensile and compressive pre-straining. The target level of plastic strain after the pre-straining process was equal to 11%. Two FEM models were used during the simulation of these four cases (see **Figure 3**): an axisymmetric model for cases with pre-straining in the y-axis, and a 3D model for cases with pre-straining in the x-axis. This was due to the pre-straining in the x-axis canceling the axial symmetry of the model, making it necessary to use a 3D model. Nonetheless, this model leveraged the existing symmetries of the SPT geometry in order to minimize the computing cost of the model. **The SPT specimen in the 3D model was shaped as a square instead of a circle in order to facilitate the implementation of the corresponding boundary condition to pre-strain it in the x-axis. In a similar way of pre-straining process in the y-axis, the pre-straining in the x-axis is reached deforming the width of the SPT specimen in the x-axis until reach a specific plastic strain in the material. The initial widths of the squared SPT specimen and its initial thickness were established in an iterative process with the goal of reaching a regular squared geometry and a final thickness of 0.5 mm. For the second step of the simulations the boundary conditions for ball and dies were a forced displacement and clamped positions respectively. These boundary conditions were assigned for the entire volume of each part forcing a rigid body behavior for these components.**

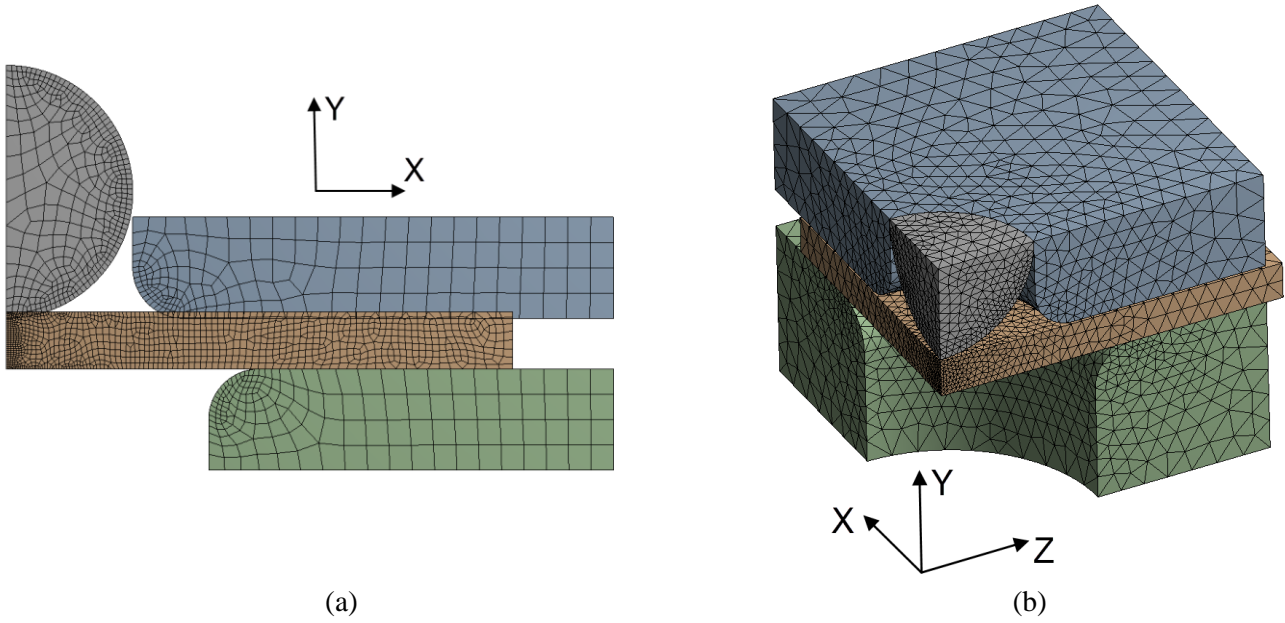


Figure 3. FEM model of the SPT: (a) axisymmetric model and (b) 3D model

After this first study, which analyzed the influence of the pre-straining in a material with a purely kinematic model (a very pronounced Bauschinger effect), a set of simulations with pre-straining were performed with an isotropic hardening model following the Ramberg-Osgood law and with the mechanical properties included in Table 1. The aim was to give an explanation to the observed behavior in the empirical investigations of Cuesta et al. (Cuesta & Alegre, 2012) and Peng et al. (Peng et al., 2019). Five simulations of the SPT were performed with tensile pre-straining levels of 0, 1, 3, 5 and 10% in the y-axis.

These two studies of pre-straining of hypothetical materials with purely kinematic model and purely isotropic model derived in the obtaining of different SPT curves. With the purpose of estimating yield strength and ultimate tensile strength from these curves, it was necessary to establish the corresponding correlation equations. In order to obtain the coefficients for these correlation equations, simulations of a set of hypothetical non-pre-strained isotropic materials were performed with the axisymmetric SPT model but excluding the pre-straining step of the simulation. Table 3 shows the selected mechanical properties of these isotropic materials, around the values included in Table 1, and the obtained parameters from their SPT curves. Table 4 represents the correlation coefficients calculated from these simulations, as well as the coefficients of determination R^2 for each regression.

Material	σ_y (MPa)	n	P_y Mao (N)	P_y CEN (N)	P_y t/10 offset (N)	$Slope_{min}$ (N/mm)
1	200	5	170.0	167.6	187.5	503.3
2	200	30	143.2	144.2	142.0	223.4
3	600	5	477.2	490.7	534.0	1525.1
4	600	30	423.3	395.2	410.0	694.9

Table 3. Mechanical properties and SPT parameters of the isotropic hypothetical materials

	α_1	α_2	β_1	R^2
Mao	0.334	-4.839	-	0.979
CEN	0.329	5.908	-	0.945
t/10 offset	0.298	20.577	-	0.915
Opt. t/10 offset	0.485	-0.145	-	0.997
Intersections method	-	-	0.202	0.991

Table 4. Correlation coefficients for the isotropic hypothetical materials

3 Results and discussion

Figure 4 shows the SPT curves obtained from the simulations with tensile and compressive pre-straining in the x and y axes, and with the Chaboche's kinematic hardening model included in Table 2. Each result was identified with the following acronyms: CF (Cold Formed), Cx (compressive pre-straining in the x-axis), Tx (tensile pre-straining in the x-axis), Cy (compressive pre-straining in the y-axis), Ty (tensile pre-straining in the y-axis) and "No CF" (non-pre-strained material). The y-axis corresponded to the SPT specimen normal axis and the x-axis corresponded to one direction contained in the specimen plane. It is observed that, according to the direction and sense of the pre-straining, the SPT curve shows different deviations from the non-pre-strained model. Specifically, the compressive pre-straining in the y-axis and the tensile pre-straining in the x-axis showed an increase in the test stiffness, being more significant for the case of pre-straining in the y-axis. By contrast, tensile pre-straining in the y-axis and compressive pre-straining in the x-axis showed a decrease in the test stiffness, being this behavior more significant in the y-axis case. In conclusion, pre-straining in the SPT specimen normal axis showed more effect in the SPT curve than the pre-straining applied along a direction contained in the specimen plane.

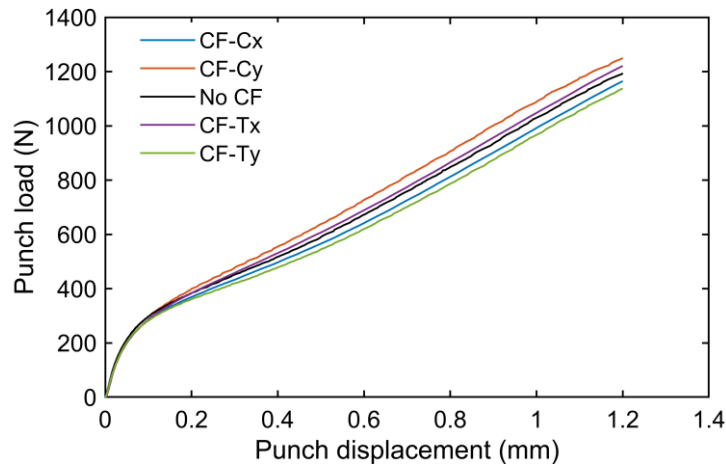


Figure 4. SPT curves of the pre-strained hypothetical materials

Table 5 includes the yield loads P_y obtained using the correlation methods for the estimation of yield strength, as well as the estimated values of yield strength using the corresponding correlation equations (see equations (1) and (2)) and the coefficients obtained in the Table 4. In order to evaluate the meaning of these estimated yield strengths, Figure 5 represents the **Von Mises** yield surfaces of the material model for the case with a tensile pre-straining of 11% in the y-axis and the non-pre-strained model (equation (9)). The strain-hardening behavior of a purely kinematic model is represented as a translation of the yield surface in the direction and sense of the stress components combination during the yielding. Considering the equation of the Chaboche's model used for this simulation (equation (10)), a tensile pre-straining of 11% in the y-axis would correspond to a tensile stress in the y-axis equal to 600 MPa approximately. It derives in a y-axis translation of the Von Mises yield surface equal to $600 - 400 = 200$ MPa. Dashed red lines of Figure 5 represent this translation.

$$(\sigma_{xx} - \sigma_{yy})^2 + (\sigma_{yy} - \sigma_{zz})^2 + (\sigma_{zz} - \sigma_{xx})^2 = 2\sigma_{y0}^2 \quad (9)$$

$$\sigma(\varepsilon_p) = \sigma_{y0} + \frac{C_1}{\gamma_1}(1 - e^{-\gamma_1\varepsilon_p}) + \frac{C_2}{\gamma_2}(1 - e^{-\gamma_2\varepsilon_p}) \quad (10)$$

From this yield surface, the new yield strength components for each direction, just after the pre-straining, can be obtained (see equation (11)). Although none of the values approaches the estimated values for each correlation method, the mean value of yield strength components of the pre-strained model ($\bar{\sigma}_y = 373.7$ MPa) was closed to the estimated

yield strengths with the SPT (Table 6 shows the normalized root-mean-square deviation (*NRMSD*) for the reference value of 373.5 MPa). This result makes sense considering the multiaxial stress field of the SPT. Consequently, all yield strength components of the pre-strained yield surface come into play to a greater or lesser extent during the test. These simulations showed that, in the absence of isotropy, the SPT estimated a mean value or equivalent isotropic value for yield strength of the material.

<i>ID</i>	P_y <i>Mao</i> (<i>N</i>)	P_y <i>CEN</i> (<i>N</i>)	P_y <i>t/10</i> <i>offset</i> (<i>N</i>)	$Slope_{min}$ (<i>N/mm</i>)	σ_y <i>Mao</i> (<i>MPa</i>)	σ_y <i>CEN</i> (<i>MPa</i>)	σ_y <i>t/10 offset</i> (<i>MPa</i>)	σ_y <i>opt. t/10</i> <i>offset</i> (<i>MPa</i>)
No CF	289.0	284.0	297.9	646.2	381.2	379.7	375.7	390.6
CF-Cy	282.9	276.6	302.7	778.6	373.1	370.0	381.4	361.4
CF-Ty	272.9	285.9	281.0	579.6	359.7	382.2	355.5	377.1
CF-Cx	281.4	283.2	284.6	606.4	371.1	378.6	359.8	376.2
CF-Tx	286.7	281.8	287.0	701.0	378.2	376.7	362.7	353.5

Table 5. SPT parameters and estimated yield strengths for the hypothetical materials

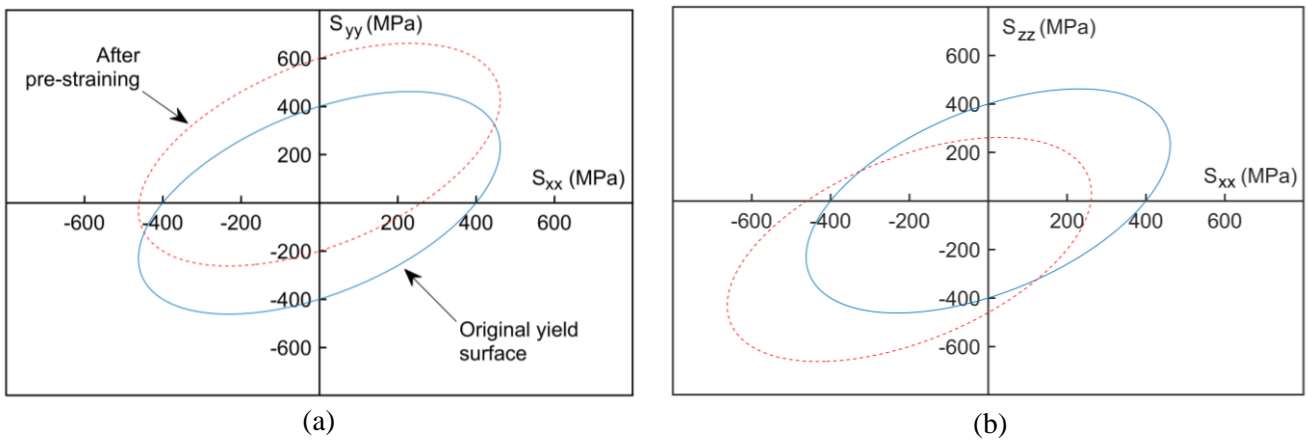


Figure 5. Sections of the yield surface evolution for the (a) xy plane and (b) xz plane

$$\begin{Bmatrix} \sigma_{cxx}^y & \sigma_{cyy}^y & \sigma_{czz}^y \\ \sigma_{txx}^y & \sigma_{tyy}^y & \sigma_{tzz}^y \end{Bmatrix} = \begin{Bmatrix} -460.5 & -200 & -460.5 \\ 260.5 & 600 & 260.5 \end{Bmatrix} \quad (11)$$

Correlation method	<i>NRMSD</i> (%)
Mao's method	1.4
CEN's method	1.0
t/10 offset method	2.5
Opt. t/10 offset method	2.2

Table 6. Normalized root-mean-square deviation (*NRMSD*) for the estimation of yield strength

Regarding the estimation of ultimate tensile strength, the maximum load method and the maximum load weighted method were not applied because of at these load levels, damage processes have been initiated in the material, and the FEM model implemented in this investigation did not include any damage model. That was the reason why this study was limited to the application of the intersections' method. Table 7 shows the intersection loads P_i obtained from the simulated SPT curves and the estimated ultimate tensile strengths with equation (5) and the correlation coefficients gathered in Table 4. Regarding ultimate tensile strength of the implemented material, it was calculated translating the true stress-strain values of equation (7) to engineering values and obtaining the maximum value of the deduced function. In this case, ultimate tensile strength of the implemented material was equal to $\sigma_u = 534.4$ MPa. Considering that the Chaboche's hardening model does not change this ultimate tensile strength with the presence of pre-straining, all the simulations should have shown similar estimations of this mechanical property. By contrast, the presence of pre-straining influenced in this estimation process, showing a *NRMSD* regarding the reference value of the non-pre-strained model ($\sigma_u = 575.9$ MPa) of 6.4%.

<i>ID</i>	P_i (N)	σ_u int (MPa)
No CF	712.7	575.9
CF-Cy	765.9	618.8
CF-Ty	658.1	531.7
CF-Cx	679.4	548.9
CF-Tx	727.7	588.0

Table 7. SPT parameters and estimated ultimate tensile strengths for the hypothetical materials

This first study has shown how the Bauschinger effect and pre-straining influence the reliability of yield strength and ultimate tensile strength estimation using a purely kinematic model as in the case of Chaboche's model. It should be noted that materials tend to show a combination of isotropic and kinematic response. It is for this reason that this study was extended for a purely isotropic hardening model in order to evaluate both behavior limits of a real material. As mentioned above, this second study implemented a hypothetical material with the mechanical properties included in Table 1 and setting an isotropic hardening model. Since this model strengthens the material homogeneously in all directions, only the pre-straining in one direction and sense (tensile pre-straining in the y-axis) was simulated. This study used four levels of plastic pre-straining: 1, 3, 5 and 10%. Figure 6 shows the SPT curves that resulted from these simulations. It was noted that, as opposed to what happens for the tensile pre-straining in the y-axis for the Chaboche's kinematic model, the SPT curve was stiffer. As the pre-straining level increased, the isotropic hardening model showed an increase in the stiffness of the SPT curve. Table 8 shows the yield loads obtained with each correlation method as well as the estimated yield strengths. It also includes the real yield strength reached after each pre-straining level, a value that was calculated with the equation of the hardening model. It is noted that all the correlation methods estimated a yield strength increment as the pre-straining level was increased, but the relative error (RE) significantly increased as pre-straining increased (see Table 9). From all correlation methods, the one that best estimated yield strength was the optimized t/10 offset method.

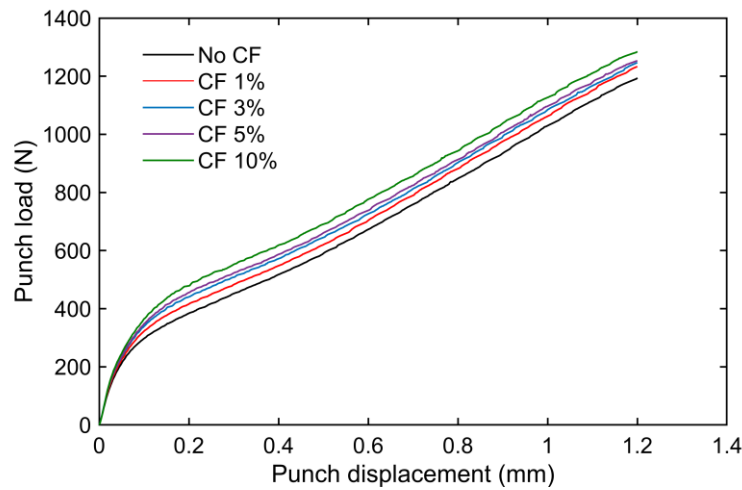


Figure 6. Parameters used in the correlation methods for yield strength estimation with the SPT

<i>ID</i>	P_y Mao (N)	P_y CEN (N)	P_y t/10 offset (N)	$Slope_{min}$ (N/mm)	σ_y Mao (MPa)	σ_y CEN (MPa)	σ_y t/10 offset (MPa)	σ_y opt. t/10 offset (MPa)	σ_y (MPa)
No CF	289.0	284.0	297.9	646.2	381.2	379.7	375.7	390.6	400
CF-1%	328.0	318.9	323.0	626.2	433.4	425.6	405.6	445.0	478
CF-3%	354.8	359.0	341.0	624.6	469.1	478.3	427.0	480.4	529
CF-5%	378.8	364.6	354.0	596.5	501.2	485.8	442.5	513.8	553
CF-10%	397.9	387.7	375.0	637.5	526.7	516.1	467.5	542.6	596

Table 8. SPT parameters and estimated yield strengths for the hypothetical materials

<i>ID</i>	RE Mao (%)	RE CEN (%)	RE t/10 offset (%)	RE opt. t/10 offset (%)
-----------	------------	------------	--------------------	-------------------------

No CF	4.7	5.1	6.1	2.4
CF-1%	9.3	11.0	15.1	6.9
CF-3%	11.3	9.6	19.3	9.2
CF-5%	9.4	12.2	20.0	7.1
CF-10%	11.6	13.4	21.6	9.0

Table 9. Relative error (*RE*) for the estimated yield strengths for the hypothetical materials

Figure 7 shows the correlation between the SPT parameters obtained from each method and the real yield strength reached after each pre-straining (from 0 to 10% of plastic pre-straining; marked with blue circles). It also shows the correlation equations previously obtained for other hypothetical materials (Table 4). Cuesta et al. (Cuesta & Alegre, 2012) and Peng et al. (Peng et al., 2019) pointed out empirically that pre-strained materials considerably differed from the correlation equations deduced for non-pre-strained materials, showing a greater slope in their correlation. It is worth noting that these differences were more pronounced for the application of the $t/10$ offset method and less accentuated for the optimized $t/10$ offset method, being the Mao's and CEN's methods in intermediate positions.

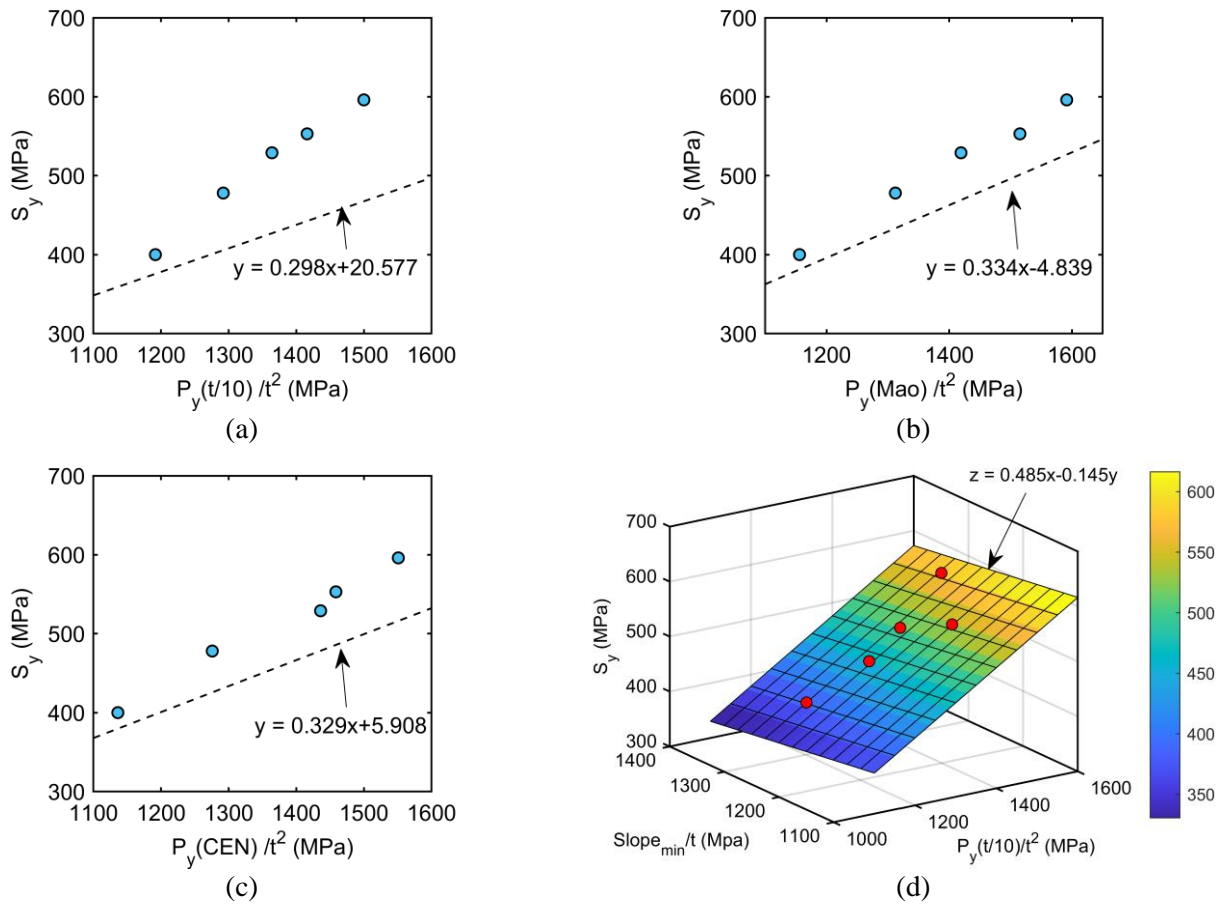


Figure 7. Application of correlation methods for the estimation of the yield strength for hypothetical materials with isotropic strain hardening and different levels of pre-straining: (a) $t/10$ offset method, (b) Mao's method, (c) CEN's method and (d) optimized $t/10$ offset method

The mechanical reason for this behavior is observed when considering the remaining hardening capability that the material has when it is tested. Figure 8 shows the stress-plastic strain curves of the evaluated material and for the different pre-straining levels. As greater pre-straining level are achieved, the material shows lower hardening rates (stress-strain slope) for a similar increment of the plastic strain during the SPT. From a Ramberg-Osgood model point of view, this would be equivalent to a hardening coefficient n that would increase as pre-straining increases. Considering this fact, in a previous investigation of Calaf-Chica et al. (Calaf-Chica et al., 2019) it was found that correlation methods for the estimation of yield strength showed a dependency with the strain-hardening capability of the material. The greater the hardening coefficient n , the higher slope of the corresponding correlation equation. In addition, as previously deduced, the higher is pre-straining, the higher is n . Thus, greater slope in the correlation

equation would be a consequence of materials combination with hardening coefficients n in ascending order. This fact is shown in Figure 9 that represents: (1) the correlation with the $t/10$ offset method of different pre-straining levels of the isotropic material with $n = 10$ (marked as red circles); (2) the application of the $t/10$ offset method in three SPT simulations of hypothetical materials with $n = 10$ and yield strengths of 400, 500 and 600 MPa (all of them without pre-straining (diamond symbols)); (3) and the application of the $t/10$ offset method for three hypothetical materials without strain-hardening capability ($n = \infty$) and yield strengths of 400, 500 and 600 MPa (square symbols). It was noted that simulations with pre-straining go from locations closed to correlation tendency of materials with $n = 10$ to the linear tendency of materials without hardening capability ($n = \infty$). Thus, changes in the correlation coefficients originated by pre-straining (and mentioned in different empirical studies (Cuesta & Alegre, 2012; Peng et al., 2019)) would come from dependency of the correlation methods not just with yield strength, but also with the strain-hardening capability. Considering that the optimized $t/10$ offset method was designed considering this dual dependency with the strain-hardening coefficient, which is the reason why this correlation method was the one that best estimated yield strength in this study.

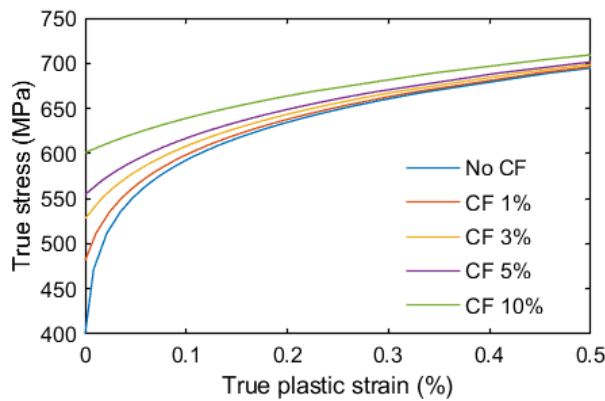


Figure 8. Parameters used in the correlation methods for yield strength estimation with the SPT

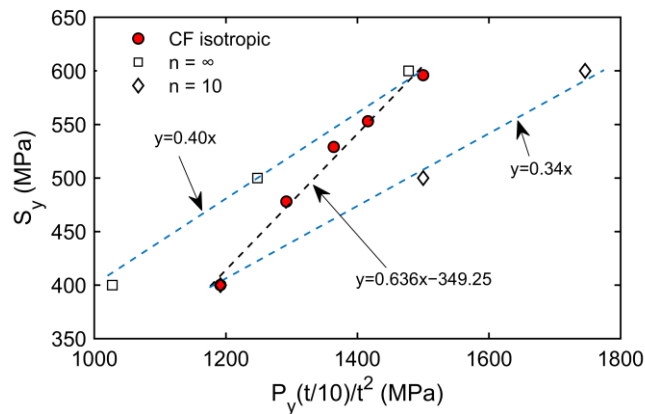


Figure 9. Parameters used in the correlation methods for yield strength estimation with the SPT

4 Conclusions

As a result of this investigation we may conclude the following:

- (a) The existence of pre-straining in a material that shows a marked Bauschinger effect derives a yield strength estimation with the SPT near a mean value of yield strength components after pre-straining.
- (b) Materials with cold pre-straining and with a marked Bauschinger effect must not be used to deduce or calculate the coefficients of the correlation equations for yield strength estimation with the SPT.

- (c) Materials with a marked isotropic behavior (non-significant Bauschinger effect) and with different pre-straining levels must not use the $t/10$ offset method, because of its marked dependency on the remaining hardening capability of the material. In any case, it is recommended to use the optimized version of the $t/10$ offset method. Mao's and CEN's methods show less dependence on strain-hardening than the $t/10$ offset method, but it should be considered that a combination of materials with different strain-hardening capabilities (different n 's) would increase the correlation deviation and reliability of these estimation methods.
- (d) The intersections' method for the estimation of ultimate tensile strength shows a slight dependency on the presence of pre-straining in the SPT specimen with a $NRMSD \approx 6\%$ for the analyzed cases.

5 Data availability

The raw/processed data required to reproduce these findings cannot be shared at this time as the data also forms part of an ongoing study.

6 References

- Abendroth, M., & Kuna, M. (2003). Determination of deformation and failure properties of ductile materials by means of the small punch test and neural networks. *Computational Materials Science*, 28(3-4 SPEC. ISS.), 633–644. <https://doi.org/10.1016/j.commatsci.2003.08.031>
- Altstadt, E., Houska, M., Simonovski, I., Bruchhausen, M., Holmström, S., & Lacalle, R. (2018). On the estimation of ultimate tensile stress from small punch testing. *International Journal of Mechanical Sciences*, 136, 85–93. <https://doi.org/10.1016/j.ijmecsci.2017.12.016>
- Bruchhausen, M., Altstadt, E., Austin, T., Dymacek, P., Holmström, S., Jeffs, S., Lacalle, R., Lancaster, R., Matocha, K., & Petzova, J. (2018). European standard on small punch testing of metallic materials. *Ubiquity Proceedings*, 1(S1), 11. <https://doi.org/10.5334/uproc.11>
- Bruchhausen, M., Holmström, S., Simonovski, I., Austin, T., Lapetite, J. M., Ripplinger, S., & de Haan, F. (2016). Recent developments in small punch testing: Tensile properties and DBTT. *Theoretical and Applied Fracture Mechanics*, 86, 2–10. <https://doi.org/10.1016/j.tafmec.2016.09.012>
- Calaf-Chica, J., Bravo Díez, P. M., Preciado Calzada, M., & Ballorca-Juez, D. (2019). A systematic FEM analysis of the influence of mechanical properties in the reliability of the correlation methods in the small punch test. *International Journal of Mechanical Sciences*, 153–154, 299–309. <https://doi.org/10.1016/j.ijmecsci.2019.02.013>
- Calaf-Chica, J., Bravo Díez, P. M., Preciado Calzada, M., & Garcia-Tarrago, M. J. (2020). Optimization of the $t/10$ offset correlation method to obtain the yield strength with the Small Punch Test. *Journal of Nuclear Materials*, 534, 152177. <https://doi.org/10.1016/j.jnucmat.2020.152177>
- Calaf Chica, J., Bravo Díez, P. M., & Preciado Calzada, M. (2017). Improved correlation for elastic modulus prediction of metallic materials in the Small Punch Test. *International Journal of Mechanical Sciences*, 134C, 112–122. <https://doi.org/10.1016/j.ijmecsci.2017.10.006>
- Campitelli, E. N., Spätig, P., Bertsch, J., & Hellwig, C. (2005). Assessment of irradiation-hardening on Eurofer97' and Zircaloy 2 with punch tests and finite-element modeling. *Materials Science and Engineering A*, 400–401(1-2 SUPPL.), 386–392. <https://doi.org/10.1016/j.msea.2005.02.088>
- CEN Workshop Agreement. (2006). Small Punch Test Method for Metallic Materials. In *Small Punch Test Method for Metallic Materials*. https://www.nen.nl/pdfpreview/preview_114589.pdf
- Cuesta, I. I., & Alegre, J. M. (2012). Hardening evaluation of stamped aluminium alloy components using the Small Punch Test. *Engineering Failure Analysis*, 26, 240–246. <https://doi.org/10.1016/j.engfailanal.2012.06.004>
- Gao, T., Ying, L., Hu, P., Han, X., Rong, H., Wu, Y., & Sun, J. (2020). Investigation on mechanical behavior and plastic damage of AA7075 aluminum alloy by thermal small punch test: Experimental trials, numerical analysis. *Journal of Manufacturing Processes*, 50, 1–16. <https://doi.org/10.1016/j.jmapro.2019.12.012>
- Guan, K., Hua, L., Wang, Q., Zou, X., & Song, M. (2011). Assessment of toughness in long term service CrMo low alloy steel by fracture toughness and small punch test. *Nuclear Engineering and Design*, 241(5), 1407–1413. <https://doi.org/10.1016/j.nucengdes.2011.01.031>
- Hähner, P., Soyarslan, C., Gülçimen Çakan, B., & Bargmann, S. (2019). Determining tensile yield stresses from Small Punch tests: A numerical-based scheme. *Materials and Design*, 182, 107974. <https://doi.org/10.1016/j.matdes.2019.107974>

- Hurst, R., Li, Y., & Turba, K. (2019). Determination of fracture toughness from the small punch test using circular notched specimens. *Theoretical and Applied Fracture Mechanics*, 103, 102238. <https://doi.org/10.1016/j.tafmec.2019.102238>
- Husain, A., Sehgal, D. K., & Pandey, R. K. (2004). An inverse finite element procedure for the determination of constitutive tensile behavior of materials using miniature specimen. *Computational Materials Science*, 31(1–2), 84–92. <https://doi.org/10.1016/j.commatsci.2004.01.039>
- Kim, M. C., Oh, Y. J., & Lee, B. S. (2005). Evaluation of ductile-brittle transition temperature before and after neutron irradiation for RPV steels using small punch tests. *Nuclear Engineering and Design*, 235(17–19), 1799–1805. <https://doi.org/10.1016/j.nucengdes.2005.05.014>
- Koga, Y., Arao, Y., & Kubouchi, M. (2020). Application of small punch test to lifetime prediction of plasticized polyvinyl chloride wire. *Polymer Degradation and Stability*, 171, 109013. <https://doi.org/10.1016/j.polymdegradstab.2019.109013>
- Kumar, J. G., & Laha, K. (2017). Localized creep characterization of 316LN stainless steel weld joint using Small Punch Creep test. *Materials Science and Engineering A*, 705, 72–78. <https://doi.org/10.1016/j.msea.2017.08.062>
- Li, H., Chen, H., Al-Abedy, H. K., & Sun, W. (2020). Study on the Fracture Mechanism of the P91 Steel During Small Punch Tensile Testing. In *Structural Integrity* (Vol. 16, pp. 106–111). https://doi.org/10.1007/978-3-030-47883-4_19
- Ma, Y. W., & Yoon, K. B. (2010). Assessment of tensile strength using small punch test for transversely isotropic aluminum 2024 alloy produced by equal channel angular pressing. *Materials Science and Engineering A*, 527(16–17), 3630–3638. <https://doi.org/10.1016/j.msea.2010.02.057>
- Mao, X., & Takahashi, H. (1987). Development of a further-miniaturized specimen of 3 mm diameter for tem disk (ϕ 3 mm) small punch tests. *Journal of Nuclear Materials*, 150(1), 42–52. [https://doi.org/10.1016/0022-3115\(87\)90092-4](https://doi.org/10.1016/0022-3115(87)90092-4)
- Okada, A., Hamilton, M. L., & Garner, F. A. (1991). Microbulge testing applied to neutron irradiated materials. *Journal of Nuclear Materials*, 179–181(PART 1), 445–448. [https://doi.org/10.1016/0022-3115\(91\)90120-V](https://doi.org/10.1016/0022-3115(91)90120-V)
- Okuda, N., Kasada, R., & Kimura, A. (2009). Statistical evaluation of anisotropic fracture behavior of ODS ferritic steels by using small punch tests. *Journal of Nuclear Materials*, 386–388(C), 974–978. <https://doi.org/10.1016/j.jnucmat.2008.12.265>
- Peng, J., Li, K., Dai, Q., Gao, G., Zhang, Y., & Cao, W. (2019). Estimation of mechanical strength for pre-strained 316L austenitic stainless steel by small punch test. *Vacuum*, 160, 37–53. <https://doi.org/10.1016/j.vacuum.2018.11.015>
- Rasche, S., Strobl, S., Kuna, M., Bermejo, R., & Lube, T. (2014). Determination of Strength and Fracture Toughness of Small Ceramic Discs Using the Small Punch Test and the Ball-on-three-balls Test. *Procedia Materials Science*. <https://doi.org/10.1016/j.mspro.2014.06.156>
- Simonovski, I., Baraldi, D., Holmström, S., Altstadt, E., Delville, R., & Bruchhausen, M. (2018). Determining the ultimate tensile strength of fuel cladding tubes by small punch testing. *Journal of Nuclear Materials*, 509, 620–630. <https://doi.org/10.1016/j.jnucmat.2018.07.041>
- Turba, K., Hurst, R. C., & Hähner, P. (2012). Anisotropic mechanical properties of the MA956 ODS steel characterized by the small punch testing technique. *Journal of Nuclear Materials*, 428(1–3), 76–81. <https://doi.org/10.1016/j.jnucmat.2011.08.042>
- Wang, L. Y., Zhou, Z. J., Li, C. P., Chen, G. F., & Zhang, G. P. (2019). Comparative investigation of small punch creep resistance of Inconel 718 fabricated by selective laser melting. *Materials Science and Engineering A*, 745, 31–38. <https://doi.org/10.1016/j.msea.2018.12.083>
- Wang, W., Zhong, J., Zhang, X., Jiang, T., & Guan, K. (2020). Study of estimation of ductile-brittle transition temperature using U-notched small punch test specimens. *Theoretical and Applied Fracture Mechanics*, 108, 102627. <https://doi.org/10.1016/j.tafmec.2020.102627>